2017 IEEE Conference on Control Technology and Applications (CCTA)
August 27-30, 2017. Kohala Coast, Hawai'i, USA

Optimal control of a wave energy converter

R. W. M. Hendrikx[1], J. Leth[2] P. Andersen[2] and W. P. M. H. Heemels[1]

Abstract— **The optimal control strategy for a wave energy converter (WEC) with constraints on the control torque is investigated. The goal is to optimize the total energy delivered to the electricity grid. Using Pontryagin's maximum principle, the solution is found to be singular-bang. Using higher order conditions, the optimal control on the singular arc is found as a function of the state and costate trajectories. Furthermore, it is shown that the transitions between bang and singular subarcs are discontinuous. Based on these findings the results of a numerical direct method are validated. Finally, the optimal control is used to benchmark an existing MPC strategy. It is found that for active control torque constraints the MPC strategy does not result in the discontinuous singular-bang transitions. However, the difference in harvested power is small.**

I. Introduction

Besides well-known clean energy resources such as wind and solar energy, the concept of wave energy conversion (WEC) has been studied in Denmark over the past 25 years [1]. WEC represents a variety of methods to extract energy from the motion of seawaves, see [2], [3] for a survey. One of the methods to convert wave motion into energy is by using a point absorber. A working prototype of a multiple point absorber has been made by the Wave Star company [4]. The point absorber principle uses a float that is attached to a hinged arm. The motion of the float caused by the wave forces is converted into energy using hydraulic coupling to a power take off (PTO) system (see e.g. [5]). This PTO system is capable of applying a variable torque to the point absorber arm, such that work is extracted from the wave motion. The control challenge is to determine this torque signal, such that the extracted work, and thereby the energy delivered to the grid, is maximized.

Various control methods for point absorbers in general have been investigated, ranging from simple methods, such as latching control [6], to more advanced methods, such as MPC [3], [7]. It has been shown in [8] that to optimize work for harmonic wave motion, the PTO system must at certain time intervals deliver work to the point absorber. This leads to the well-known *reactive* control-scheme, in which the power is reversed during the reactive part of the control strategy, to optimize power production during the active part. Furthermore, the optimal control strategy without torque constraints has been investigated by Nielsen et al. for irregular sea waves in [9] by using Pontryagin's maximum principle, leading to a noncausal control strategy. This strategy was modified by Nielsen et al. to obtain an implementable suboptimal strategy.

The system model and control problem presented in this paper are closely related to what is presented in [10], [11], [12]. However, the cost in [10] includes an interior (state) penalty term and singular solutions are not addressed. In [11] a slightly different control structure is studied for which no singular solution exists. In [12] the radiation force is simplified yielding a singular-bang solution with an explicit control law given in terms of states only. In this paper the radiation force is expressed as the output of a state space realization which, as in [12], also yield a singular-bang solution but where the control law now depends explicit on costates. Also switching times are determined in [12], whereas transition between singular and bang solutions is addressed in this paper.

Finally, in [13] an MPC strategy for optimal motion of a wave energy converter is studied and compared to theoretical upper bounds.

For the Wave Star machine, research strategies including reactive control and MPC have been investigated. The reactive control scheme is based on regular wave theory that does not include knowledge about future wave torques. Aiming to optimize energy delivered to the grid and also taking into account losses in the power conversion, Andersen et al. [14] compared this scheme to an MPC strategy. This MPC strategy optimizes the harvested energy for a finite horizon of future predicted wave torques. They showed that an input-constrained MPC strategy can outperform the reactive controller. A state observer was used to estimate the future states of both the system and the wave. This paper aims to derive an open-loop optimal control strategy for a linearized model of the Wave Star point absorber. Both pure sine wave excitation forces and realistic measured excitation forces represented by sea states are used. This optimal control strategy will provide insight into the nature of the optimal control problem and the direction of the power flow in the presence of control torque constraints. Furthermore, the optimal control signal and the resulting energy will be used to assess performance of the MPC strategy derived by Andersen et al.

To solve the optimal control problem, first a linearized model as used in [14] will be obtained. Using this model, the necessary conditions for optimality based on Pontryagin's maximum principle (PMP) will be stated. It will be shown that the nature of the model and the presence of

[1]Bob Hendrikx and Maurice Heemels are with the Control Systems Technology Group, Department of Mechanical Engineering, Eindhoven University of Technology, Eindhoven, 5600 MB, The Netherlands r.w.m.hendrikx@student.tue.nl, m.heemels@tue.nl

[2]John Leth and Palle Andersen are with the Department of Electronic Systems, Automation & Control, Aalborg University, 9220 Aalborg East Denmark jjl,pa@es.aau.dk

constraints on the PTO torque will result in the optimal control input containing either bang or singular trajectories, or a combination of both. A characterization of the optimal control on these singular trajectories will be obtained by resorting to higher order conditions. A solution for the case where control constraints are not active will be obtained as a function of initial state and wave excitation force. For the case where constraints are active, we will show that transitions from bang trajectories to singular trajectories will be discontinuous, based on the work of McDanell and Powers [15]. Since it is very difficult to obtain closed form solutions in the singular-bang case, we will obtain a numeric solution by solving the optimal control problem using a *direct* approach via the Matlab solver package ICLOCS [16]. The resulting control trajectory will be discussed and compared to the MPC strategy for different wave profiles. Finally, conclusions will be drawn regarding usefulness of the optimal control for real implementation, performance of the MPC strategy and possible future research questions.

II. System model and objective function

As in [14], a simplified linear model of the point absorber is used. The arm of the point absorber is shown in Figure 1.

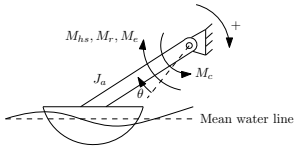

Fig. 1. Schematic depiction of the point absorber model and the moments caused by water forces and control torque.

We denote the arm angle by θ and the angular velocity and acceleration by $\omega = \dot{\theta}$ and $\dot{\omega}$, respectively. The arm is characterized by its moment of inertia and the equation of motion is given by

$$J_a\dot{\omega} = M_{hs} + M_r + M_e - M_c, \tag{1}$$

where M_{hs} denotes the hydrostatic force moment (HsFM), M_r the radiation force moment, M_e the external moment caused by the wave profile and M_c the control moment. For parameter values used in the sequel see Table I below.

The hydrostatic force moment is the moment caused by the static force of the water pressure on the float with respect to the mean water line (Archimedes' law). It depends nonlinearly on θ, however, a linearized relation is used in [14] of the form

$$M_{hs} = -k_h\theta. \tag{2}$$

The radiation force moment is caused by the forces acting on the float as it moves through the water, experiencing friction and water inertia. It is a function of ω and $\dot{\omega}$ and can be described by the relation [17]

$$M_r = -J_{h\infty}\dot{\omega} - \int_0^t h_r(t-\tau)\omega(\tau)d\tau, \tag{3}$$

where the impulse response h_r is determined numerically using a boundary-element method [18]. A transfer function can then be identified for the convolution part and represented by a state space realization of the form

$$\dot{x}_r = A_r x_r + B_r\omega \tag{4a}$$
$$M_r = -J_{h\infty}\dot{\omega} + C_r x_r \tag{4b}$$

with system matrices (^{T} indicate transpose)

$$A_r = \begin{bmatrix} 0 & 1 & 0 \\ 0 & 0 & 1 \\ -a_0 & -a_1 & -a_2 \end{bmatrix},\ B_r = \begin{bmatrix} 0 \\ 0 \\ 1 \end{bmatrix},\ C_r = \begin{bmatrix} c_1 \\ c_2 \\ c_3 \end{bmatrix}^T.$$

Introducing the moment of inertia $J = J_a + J_{h\infty}$ and combining (1), (2) and (4) yields

$$\dot{\omega} = \frac{-k_h}{J}\theta + \frac{1}{J}C_r x_r + \frac{1}{J}M_e - \frac{1}{J}M_c \tag{5a}$$
$$\dot{x}_r = A_r x_r + B_r\omega, \tag{5b}$$

which can be rewritten in state space form

$$\begin{bmatrix} \omega \\ \dot{\omega} \\ \dot{x}_r \end{bmatrix} = \left[\begin{array}{cc|c} 0 & 1 & 0 \\ \frac{-k_h}{J} & 0 & \frac{1}{J}C_r \\ \hline 0 & B_r & A_r \end{array}\right] \begin{bmatrix} \theta \\ \omega \\ x_r \end{bmatrix} + \begin{bmatrix} 0 \\ -\frac{1}{J} \\ 0 \end{bmatrix} M_c(t) + \begin{bmatrix} 0 \\ \frac{1}{J} \\ 0 \end{bmatrix} M_e(t), \tag{6}$$

or more compactly

$$\dot{x}(t) = Ax(t) + Bu(t) + \Gamma\gamma(t), \tag{7}$$

where $x_1 = \theta$, $x_2 = \omega$, $x_{i+2} = x_{ri}$, $i = 1,2,3$, the input $u(t)$ is used for the control moment $M_c(t)$ and the external wave moment $M_e(t)$ is captured in the signal $\gamma(t)$.

The objective of the optimal control strategy is to maximize the power that is delivered to the grid. To obtain this power, it is assumed that the arm of the point absorber is connected to an ideal generator through a shaft that is viscously damped. This is shown in Figure 2.

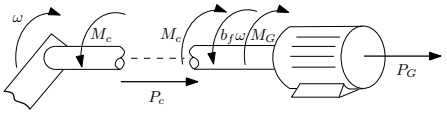

Fig. 2. Modeling of generator efficiency with friction loss term $-b_f\omega$ on the generator shaft. The generated power P_G equals the power flow due to the control torque ($P_c = M_c\omega$) minus the friction power loss.

The (instantaneous) power that is generated equals the power taken off by the control torque $P_c = M_c\omega$, minus the friction power loss ($P_f = M_f\omega$), where $M_f = b_f\omega$. The generated power, $P = P_G$ becomes

$$P = M_G\omega = P_c - P_f = (M_c - b_f\omega)\omega = u\omega - b_f\omega^2. \tag{8}$$

The objective is to maximize the energy delivered to the grid, which is the integral of the power P. The objective function that is to be maximized over a wave sequence of length t_f becomes

$$\int_0^{t_f} Pdt = \int_0^{t_f} \big(u(t)\omega(t) - b_f\omega^2(t)\big)dt. \tag{9}$$

Where the constraint on the control torque has to be satisfied:

$$u_{\min} \le u \le u_{\max}, \tag{10}$$

with $u_{\max} = -u_{\min} = 2\times 10^6$ [Nm].

Parameter	Value	Units	Description
J_a	6.36×10^6	kgm^2	Arm moment of inertia
J_∞	3.31×10^6	kgm^2	Water moment of inertia
k_h	29.9×10^6	Nm/rad	HsFM stifness
b_f	2.1	Nms/rad	PTO friction loss coefficient
a_0	9.188	-	Impulse response parameter
a_1	10.76	-	Impulse response parameter
a_2	4.702	-	Impulse response parameter
c_1	6.003×10^{-4}	-	Impulse response parameter
c_2	2.934×10^7	-	Impulse response parameter
c_3	1.013×10^7	-	Impulse response parameter

TABLE I

PARAMETERS USED IN THE LINEARIZED STATE SPACE MODEL OF THE POINT ABSORBER.

III. OPTIMAL CONTROL PROBLEM AND PONTRYAGIN'S MAXIMUM PRINCIPLE

Using Pontryagin's maximum principle (PMP) it will be shown that the optimal solution is to either saturate the control (bang) or follow a singular trajectory. Moreover, a feedback expression will be derived for the control on the singular trajectory and used to obtain the optimal control for a case without input constraints. Finally, the behavior at transitions between singular and bang trajectories will be analyzed. The results obtained will be used to validate the numerical solutions obtained in Section IV.

For given initial condition x_0, external wave moment $\gamma = \gamma(t)$ and final time t_f, we summarize the optimal control problem (in Lagrange form) from Section II:

$$\max_u \int_0^{t_f} P(x,u)dt, \tag{11a}$$

subject to the dynamics:

$$\dot{x} = Ax + Bu + \Gamma\gamma, \quad x(0) = x_0 \tag{11b}$$

and the constraint

$$u_{\min} \le u \le u_{\max}. \tag{11c}$$

In the sequel, let u^* denote a solution to the optimal control problem (11), and x^* the corresponding solution to (11b). Moreover, for a function f depending on u and/or x we write f^* to indicate that f should be evaluated along the optimal solution u^* and/or x^*.

A. Singular arcs

The Hamiltonian is

$$\begin{aligned} \mathscr{H}(x,u,\lambda,t) &= P(x,u) + \lambda^T\left(Ax + Bu + \Gamma\gamma\right) \\ &= (x_2 + \lambda^T B)u - b_f x_2^2 + \lambda^T(Ax + \Gamma\gamma) \\ &\triangleq \Phi(x,\lambda)u + \Theta(x,\lambda,t), \end{aligned} \tag{12}$$

with switching function (b_2 - the second entry in B)

$$\Phi(x,\lambda) = x_2 + b_2\lambda_2 \qquad (= \omega + b_2\lambda_2), \tag{13}$$

and $\lambda \in \mathbb{R}^5$ the costate determined by the Cauchy problem

$$\begin{aligned} \dot{\lambda} &= -\mathscr{H}_x^*, \quad \lambda(t_f) = 0 \\ &= -A^T\lambda + B_1 u^* + B_2 P_2 x^*, \quad \lambda(t_f) = 0, \end{aligned} \tag{14}$$

where $\mathscr{H}_x = \frac{\partial \mathscr{H}}{\partial x}$, P_2 is the projection onto the second coordinate, $B_1 = -P_2^T$ and $B_2 = -2b_f B_1$.

The input that maximizes the Hamiltonian is thus

$$u = \begin{cases} u_{\max}, & \text{if } \Phi^* > 0 \\ u_{\min}, & \text{if } \Phi^* < 0 \\ \text{singular}, & \text{if } \Phi^* = 0 \end{cases}, \tag{15}$$

which indicates that the PMP provides no information if $\mathscr{H}_u^* = \Phi^* \equiv 0$ on some interval $[t_1, t_2]$. If an optimal control exists on this interval, it is called a *singular arc*. For the control to be optimal in this case, it is necessary that the *Generalized Legendre-Clebsch* (GLC) condition holds [19]: On an optimal singular subarc of order q, it is necessary that

$$(-1)^q \frac{\partial}{\partial u}\left(\frac{d^{2q}}{dt^{2q}}\mathscr{H}_u^*\right) \le 0 \tag{16}$$

where the order of a singular arc is defined as the smallest integer q, for which the input appears explicitly in the expression

$$\frac{d^{2q}}{dt^{2q}}\mathscr{H}_u^* = \frac{d^{2q}}{dt^{2q}}\Phi^*, \tag{17}$$

with a coefficient that is not identically zero on $[t_1, t_2]$.

As the * notation can be very cumbersome we henceforth follow common practices and suppress it.

B. Feedback on the singular arc

The control law on a singular arc can be determined by the demand that the solution must stay on the singular arc (i.e. $\mathscr{H}_u = \Phi = 0$ for all $t \in [t_1, t_2]$) . Hereto we take the time derivatives of $\mathscr{H}_u$ until the input appears explicitly. It can be shown that the input only first appears explicitly in the time derivatives for even values of q (see [15]). We have

$$\begin{aligned} \dot{\mathscr{H}}_u &= \dot{x}_2 + B^T\dot{\lambda} \\ &= P_2[Ax + Bu + \Gamma\gamma(t)] + B^T[-A^T\lambda + B_1 u + B_2 P_2 x] \\ &= (P_2 A + B^T B_2 P_2)x - B^T A^T\lambda + P_2\Gamma\gamma(t) \end{aligned} \tag{18}$$

$$\begin{aligned} \ddot{\mathscr{H}}_u &= (P_2 A + B^T B_2 P_2)(Ax + Bu + \Gamma\gamma(t)) \\ &\qquad - B^T A^T(-A^T\lambda + B_1 u + B_2 P_2 x) + P_2\Gamma\dot{\gamma}(t) \\ &\triangleq \alpha u + \beta(x,\lambda,t) = 0, \end{aligned} \tag{19}$$

where

$$\alpha = \frac{\partial}{\partial u}\ddot{\mathscr{H}}_u = (P_2 A + B^T B_2 P_2)B - B^T A^T B_1. \tag{20}$$

By substitution of the numerical values in Table I we obtain $\alpha = 0.064$, verifying that the GLC condition (16) holds (with $q = 1$). Hence, the input necessary to maintain singularity is

$$u = -\alpha^{-1}\beta(x,\lambda,t), \tag{21}$$

which, from the definition of β, can be written as a linear feedback in state x, costate λ and external inputs $\gamma, \dot{\gamma}$

$$u = -\alpha^{-1}\beta(x,\lambda,t) \triangleq K_1 x + K_2\lambda + K_3\gamma(t) + K_4\dot{\gamma}(t), \tag{22}$$

with (using u in [MNm])

$$K_1 = [-29.9\ 92.2\ -214.3\ -280.3\ -52.2], \quad K_3 = 1,$$
$$K_2 = [0\ -9.5\ 0\ 2.3\ -10.8], \quad K_4 = -2.3024,$$

using the values from Table I. Substitution of the feedback law (22) in the system dynamics (11b) and the costate dynamics (14) yields a two-point boundary value problem (TPBVP), where the initial state x_0 and the final costate $\lambda(t_f) = 0$ are fixed.

For the wave excitation moment $\gamma(t) = 0.4 \times 10^6 \sin(t)$ the Matlab shooting function `bvp4c.m` has been used to solve the TPBVP, resulting in Figure 3. As an indication of correctness, we show the two terms that make up the switching function (13). The coinciding of these terms implies that the resulting trajectory is fully singular.

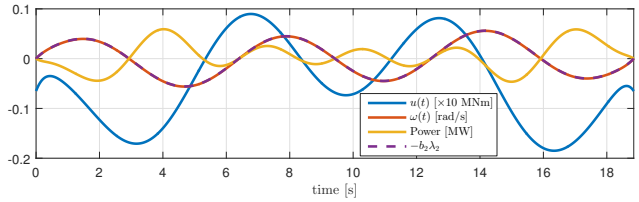

Fig. 3. The trajectories resulting from solving the TPBVP with the shooting algorithm `bvp4c.m`.

So far we have been looking at singular solutions only. In general, optimal solutions will consist of both bang and singular sub-arcs. We now investigate the transition between these two types of sub-arcs.

C. Optimal control at singular-bang junctions

Solving the TPBVP for the optimal control problem (11) is, in general, very difficult since it is not known beforehand at what times the switch between bang and singular arcs should occur. However, it was shown by McDanell and Powers [15] that if u is an optimal control containing both nonsingular subarcs and piecewise continuous, qth order singular subarcs, it holds that (superscript indicating order of time derivative)

(i) If $\mathscr{H}_u^{2q} \neq 0$ on the nonsingular side of a junction, then the control is discontinuous.

(ii) If $\beta = 0$, $\alpha \neq 0$ (as defined in (19)) and $u_{\min}, u_{\max} \neq 0$ at a junction, then the control is discontinuous.

(iii) If u is piecewise continuous on the singular subarc, $\mathscr{H}_u^{2q} = 0$ on the nonsingular side of a junction and $\alpha \neq 0$ at the junction, then the control is continuous.

To show that the switching is discontinuous at a junction, we will show that condition (i) holds without solving the optimal control problem (11) explicitly. In the sequel, we consider external wave moments of the form $\gamma = \hat{\gamma}\sin(at + \phi)$, see however Remark 1 below. These external moments can be regarded as outputs of the exosystem

$$\dot{x}_e = A_e x_e, \quad \gamma = C_e x_e, \quad A_e = \begin{bmatrix} 0 & 1 \\ -a^2 & 0 \end{bmatrix}, \quad C_e = \begin{bmatrix} 1 & 0 \end{bmatrix}, \tag{23}$$

for suitable initial condition $x_e(0) = (\hat{\gamma}\sin(\phi), \hat{\gamma}a\cos(\phi))$. We add the exosystem to the system dynamics (11b), to form the wave-autonomous system $(\tilde{A}, \tilde{B})$

$$\dot{\tilde{x}} = \tilde{A}\tilde{x} + \tilde{B}u, \quad \tilde{A} = \left[\begin{array}{c|c} A & \Gamma C_e \\ \hline 0 & A_e \end{array}\right], \quad \tilde{B} = \left[\begin{array}{c} B \\ \hline 0 \end{array}\right]. \tag{24}$$

For this system we can again form the Hamiltonian, in a way similar to (12), where the explicit input $\gamma(t)$ is now left out as it is generated within the system itself. Extending the matrices B_1, B_2, P_2 used in (19) with two zero entries to account for the new state $\tilde{x} \in \mathbb{R}^7$, we obtain the following

$$\begin{aligned} \ddot{\mathscr{H}}_u &= (P_2\tilde{A}\tilde{A} - \tilde{B}^T\tilde{A}^T B_2 P_2 + \tilde{B}^T B_2 P_2 \tilde{A})\tilde{x} + \tilde{B}^T\tilde{A}^T\tilde{A}^T\tilde{\lambda} \\ &\quad + (P_2\tilde{A}\tilde{B} - \tilde{B}^T\tilde{A}^T B_1 + \tilde{B}^T B_2 P_2 \tilde{B})u = 0 \end{aligned} \tag{25}$$

which is equivalent to (19), without the terms containing $\gamma, \dot{\gamma}$. Introducing the augmented state $\tilde{z} = \begin{bmatrix} \tilde{x}^T & \tilde{\lambda}^T \end{bmatrix}^T$, we can write (25) as

$$m^T\tilde{z} = k, \tag{26}$$

where

$$m = \frac{\partial}{\partial \tilde{z}}\ddot{\mathscr{H}}_u, \quad k = -\frac{\partial}{\partial u}\ddot{\mathscr{H}}_u u = -\tilde{\alpha}u, \tag{27}$$

a row vector and scalar, respectively, defined by (25). The dynamics that $\tilde{z}$ must satisfy are given by

$$\dot{\tilde{x}} = \tilde{A}\tilde{x} + \tilde{B}u \tag{28}$$
$$\dot{\tilde{\lambda}} = -\frac{\partial \mathscr{H}}{\partial \tilde{x}} = -\tilde{A}^T\lambda + B_1 u + B_2 P_2 \tilde{x}. \tag{29}$$

We write this as

$$\dot{\tilde{z}} = \tilde{F}\tilde{z} + \tilde{g}, \tag{30}$$

where

$$\tilde{F} = \begin{bmatrix} \tilde{A} & 0 \\ B_2 P_2 & -\tilde{A}^T \end{bmatrix}, \quad \tilde{g} = \begin{bmatrix} \tilde{B} \\ B_1 \end{bmatrix} u. \tag{31}$$

To verify condition (i) for $\ddot{\mathscr{H}}_u$ we assume that $\tilde{g}$ is a constant input since in this case the local optimal control satisfies one of the active constraints, i.e. $u = u_{\text{bang}} \in \{u_{\min}, u_{\max}\}$.

Now employ the state transformation

$$\zeta = \tilde{z} + \tilde{F}^{-1}\tilde{g}, \tag{32}$$

transforming (30) to a homogeneous system on a nonsingular subarc. Applying this transformation to the affine state constraint expressed by (26) as well, we obtain the expression

$$m^T\zeta = k + m^T\tilde{F}^{-1}\tilde{g}. \tag{33}$$

We show that the right-hand side of this expression is zero by observing that

$$\tilde{F}^{-1} = \left[\begin{array}{c|c} \tilde{A}^{-1} & 0 \\ \hline \tilde{A}^{-T}B_2P_2\tilde{A}^{-1} & -\tilde{A}^{-T} \end{array}\right], \tag{34}$$

leading to

$$m^T\tilde{F}^{-1}\tilde{g} = \left[P_2\tilde{A}\tilde{B} + \tilde{B}^T B_2 P_2 \tilde{B} - \tilde{B}^T\tilde{A}^T B_1\right] u, \tag{35}$$

which equals $-k$ (see (25)), thus canceling the expression for k in the right-hand side of (33). As a result, to show that condition (i) is satisfied for the optimal control problem

under consideration, it suffices to show that there exists no interval $[t_1,t_2]$ on the nonsingular side of a junction where

$$\dot{\zeta} = \tilde{F}\zeta, \quad m^T\zeta = 0, \tag{36}$$

for any allowable state $\zeta(t_1) = \zeta_{t1} \neq 0$. Hence, it is enough to show that the set of allowable states are unobservable with respect to the pair $(\tilde{F}, m^T)$. That is, a sufficient condition for (36) to have no solution is that

$$\mathscr{Z} \cap \mathscr{UO} = \varnothing \tag{37}$$

with the set of allowable states

$$\mathscr{Z} = \{\zeta \in \mathbb{R}^{14} \,|\, L\zeta \neq 0\}, \quad L = \begin{bmatrix} 0^{2\times 5} & I^{2\times 2} & 0^{2\times 7} \end{bmatrix}, \tag{38}$$

and the unobservable subspace

$$\mathscr{UO} = \{\zeta \in \mathbb{R}^{14} \,|\, O\zeta = 0\}, \quad O = \begin{bmatrix} m^T \\ m^T\tilde{F} \\ \vdots \\ m^T\tilde{F}^{n-1} \end{bmatrix}. \tag{39}$$

Using the values in Table I , a basis for the (2-dimensional) unobservable subspace is obtained[1]

$$\mathscr{UO} = \text{Range}\left\{ \begin{bmatrix} 0^{12\times 2} \\ I^{2\times 2} \end{bmatrix} \right\}, \tag{40}$$

implying that (37) holds true. Thus there can exist no interval $[t_1,t_2]$ on which $\ddot{\mathscr{H}}_u \equiv 0$, and therefore the transition between bang and singular subarcs of the optimal input must be discontinuous.

Remark 1: We only showed discontinuous transitions in the case of external wave moments on the form (23). However, the result can be extended to more general classes of external waves e.g., those composed by sinusoids, with the use of

$$A_E = diag(A_e,\ldots,A_e), \quad C_E = \begin{bmatrix} C_e & \cdots & C_e \end{bmatrix},$$
$$x_E(0) = (\hat{\gamma}_1\sin(\phi_1), \hat{\gamma}_1 a_1\cos(\phi_1), \ldots, \hat{\gamma}_k\sin(\phi_k), \hat{\gamma}_k a_k\cos(\phi_k)).$$

A further analysis of the switching times between bang and singular sub-arcs will be conducted in future work. However, the above will be used to verify that the numerical solutions obtained in the next section have the correct qualitative behavior (see e.g. [20], [21] for a discussion on methods for numerical solution of optimal control problems).

IV. Solutions from the direct method

In this section, we use a different approach from the one used in Section III. The *direct* method, also known as the *first-discretize-then-optimize* method, poses the optimal control problem as a non-linear optimization problem in the time-discretized state and input space. Multiple software packages and manual methods exist for this method (see [21]). We chose the free solver package ICLOCS [22], since it produced the most accurate results out of several options. ICLOCS is a direct solving package that uses the trapezoidal collocation method[2] in which the optimal control problem is divided into multiple intervals that are solved separately. It uses the third-party CVODE ODE solver, with an *Adams implicit integration* scheme and *Newton iteration* to generate a non-linear program. This NLP is then solved by a third-party NLP solver. ICLOCS allows the usage of both Matlab's `fmincon.m` and the third party open source solver IPOPT.

A. ICLOCS output comparison for different NLP solvers

We run a simulation for 10π seconds for an external wave moment $\gamma = 2\sin(t)$ [MNm] and the resulting input is shown in Figure 4. We used both the IPOPT solver and the `fmincon.m` solver and found that both result in different control trajectories. It can be seen in Figure 4 that with the IPOPT solver we see a jump discontinuity (blue) at singular-bang junctions, whereas with the `fmincon.m` solver the transition appears continuous. Furthermore, since ICLOCS uses an *infeasible-path* approach (see [23]), Lagrange multipliers are available for the dynamic constraints (11b). These multipliers are the discrete equivalent of the costate trajectories that appear in the indirect method and allow to check if the necessary conditions obtained in Section III hold. The singular input (red) introduced in (21) is shown as a function of the state and the Lagrange multipliers. It coincides perfectly with the singular interval for the IPOPT solver. For the `fmincon.m` this is not the case. This strongly suggests that the IPOPT output is the correct optimal control.

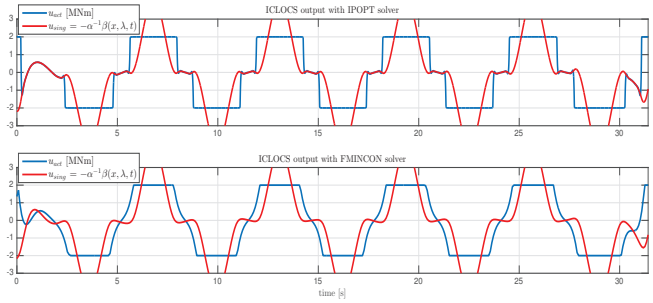

Fig. 4. The optimal control problem solved by ICLOCS with both the IPOPT and FMINCON solver. The singular input is also shown as a function of the state and Lagrange multipliers.

B. Optimal control strategy

In Figure 5 the relevant state trajectories are shown. The terms $b_2\lambda_2$ and ω that form the switching function Φ are also shown to verify the position of the singular arcs that should appear whenever $\Phi = 0$. The intervals where these terms coincide are clearly visible, again confirming that the results are as we would expect. Figure 6 shows the trajectories of $\ddot{\mathscr{H}}_u$, that are zero on the singular interval as we would expect. Furthermore, the values of $\beta(\gamma,\lambda,t)$ are shown. Interestingly, the sufficient condition (ii) discussed

[1]The unobservable modes of the system originate from the costate dynamics $-\tilde{A}^T$ in $\tilde{F}$ that contain a copy of the exosystem dynamics A_e.

[2]We stress that, while this is an advanced method aiming to solve the continuous time control problem, the MPC method explained in Section V address a sampled control system constraining the control signal to be constant between sampling instants.

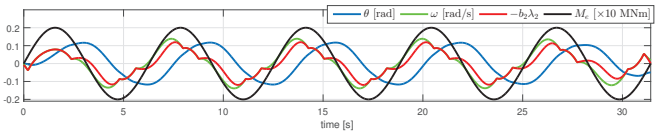

Fig. 5. The controlled response of the states θ and ω to an external wave moment $M_e = \gamma = 2\sin(t)$. The terms $b_2\lambda_2$ and ω that form the switching function Φ are added to show that the singular intervals of the control coincide perfectly with the intervals where $\Phi = 0$.

in Section III-C does not hold, as can be clearly seen from the first singular arc in the plot. Understanding the optimal

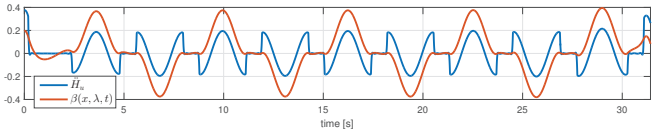

Fig. 6. Plots of the trajectories of $\ddot{H}_u$ that is zero on the singular intervals and β that is non-zero both before and on the singular intervals.

control strategy, and especially the discontinuous behavior on junctions, is a nontrivial task since the dynamics of the point absorber are complicated. We recall that for power to be delivered to the grid, the sign of u must be equal to the sign of ω. We would expect that the optimal control solution is to keep the signs equal. Figure 7 shows the power that is delivered to the grid. Clearly, in the optimal solution there are times when power is reversed and the grid is powering the point absorber. These power reversals occur whenever a switch to a singular arc occurs. The control switches discontinuously to approximately zero and the friction terms become dominant. After some time on the singular arc the control crosses a point where the angular velocity stays positive (resp. negative) and the torque becomes positive (resp. negative) again, leading to a short time of zero power. The discontinuous transition to the saturated control then again results in a short interval of power loss. It appears that this strategy, while suboptimal locally, optimizes future energy harvest. This result is in line with the findings of previous research, that the optimal strategy is to reverse power at certain times.

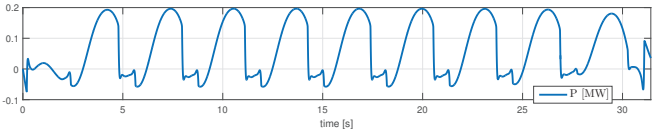

Fig. 7. The power that is generated using the optimal control torque. During the singular intervals, the generated power switches discontinuously to a singular arc in order to minimize the energy loss that is necessary for maximizing future energy harvest.

V. Comparison with MPC strategy

In this section, we will compare the optimal control solution to the MPC control solution derived by Andersen et al. in [14]. The MPC strategy uses a zero-order-hold discretized version of the system dynamics (11b), with sample time $\tau_{\text{mpc}} = 0.1$s. The optimal input sequence is calculated for a horizon of $T_{\text{mpc}} = 8$s, with $N = T_{\text{mpc}}/\tau_{\text{mpc}}$, and the first input is implemented at each time instant $t = k\tau_{\text{mpc}}$ for $k \in \mathbb{N}$, leading to

$$u_k = \operatorname{argmax} \left[\tau_{\text{mpc}} \sum_{\ell=k}^{k+N-1} \omega_{\ell+1} u_\ell - b_f \omega_{\ell+1}^2 \right], \tag{41}$$

subject to (for $\ell = k, \ldots, k+N-1$)

$$x_{\ell+1} = A_d x_\ell + B_d u_\ell + \Gamma_d \gamma_\ell, \quad u_{\min} \le u_\ell \le u_{\max}. \tag{42}$$

Where (41) is a discretized approximation of the energy generated and (42) are the discretized wave converter dynamics and the control torque constraints. The constraint optimization problem is solved for sampled time series of external wave moments γ_k, using the Matlab routine `quadprog.m`. In [14], Andersen et al. used a Kalman filter for estimating the state of the system dynamics and a wave generating model. However, wave estimation is beyond the scope of this paper and we will remove this model for the purpose of comparison. We will assume that the MPC strategy is aware of the actual wave sequence. This will make it more straightforward to find the qualitative differences between the optimal and MPC strategy.

A. Excitation moments

The three external wave moments that are used are shown in Figure 8. Two perfect sinewaves are used, where M_{e1} will have singular-bang optimal solution and M_{e2} will have a totally singular solution where no constraints are active. Furthermore, M_{e3} will consist of wave moments, generated using a stochastic Pierson-Moskowitz spectrum model, classified as sea state $S3$ as used in [14]. To reduce computational efforts, the sea state is shortened (compared to [14]) and all three wave moments will have a total simulation time of 50 seconds (compared to 650 seconds in [14]).

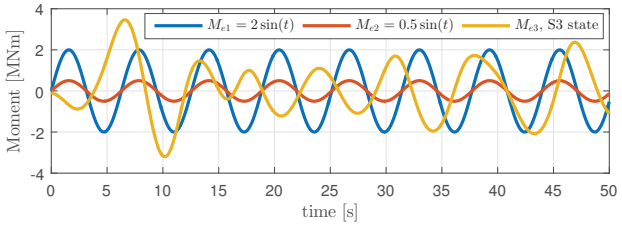

Fig. 8. Wave excitation moments that were used to compare the MPC strategy with the optimal strategy.

B. Comparison method

The average power generated in the MPC simulation is calculated by Andersen et al. using a discrete approximation:

$$W_{\text{discr}} = \tau_{\text{mpc}} \sum_{k=0}^{N-1} \omega_{k+1} u_k - b_f \omega_{k+1}^2, \tag{43}$$

$$\tilde{P}_{\text{discr}} = W_{\text{discr}}/T_{\text{mpc}}. \tag{44}$$

To compare the results from the optimal control simulations and the MPC simulations, we must account for the fact

that the energy determined by ICLOCS is more precise than this discrete approximation. Therefore, after running the total MPC simulation and obtaining the MPC input, we re-simulate the model response to the MPC input using `ode45.m`, assuming that the input is applied using zero-order hold. The cost is now integrated as an extra state, relying on the higher order integration of `ode45.m` to produce more accurate results. In the next section, we will present both the discrete power and the *continuous* power resulting from the re-simulation using `ode45.m`.

C. Comparison results

The results of the comparison are shown in Table II. The power that was produced by the optimal control input is shown in the right column. The first two columns show the power calculated as in (44), and simulated as an extra state using `ode45.m`, respectively. The numbers in parentheses correspond to the first 38 seconds, approximately corresponding to the last time a wave (M_{e1} or M_{e2}) has completed a full period without entering the last 8 seconds where the MPC horizon looks beyond the total simulation time of 50 seconds.

It can be seen that in all cases the MPC strategy performs very well and is able to harvest close to maximum energy. The relative MPC performance for the low amplitude external wave M_{e2} is 92% (86%). For the waves with higher amplitude we see that the MPC is able to harvest 98% (99%) of the optimal energy. This difference might be explained by the active constraints in the latter cases. With large regions of active constraints, the problem reduces to determining the right switching times. Whereas for the case with singular control, the strategy leaves more room for deviations from the optimal strategy. We do note however, that these results use the exact same model for the MPC and the simulation. Furthermore, the MPC has full knowledge of future wave moments. Therefore these results cannot be translated to a real wave machine. They serve merely to validate the MPC optimization approach.

	MPC, discr.	MPC, ode45.	Optimal
M_{e1} Sine, ampl. 2	60.1 (57.1)	64.5 (61.4)	65.8 (61.9)
M_{e2} Sine, ampl. 0.5	3.92 (3.52)	4.61 (4.28)	5.03 (4.95)
M_{e3} Sea state S3	43.4 (42.6)	46.0 (45.5)	46.8 (46)

TABLE II

AVERAGE PRODUCED POWER (IN [KW]) FOR THE DIFFERENT EXTERNAL WAVE MOMENTS AND THE DIFFERENT CONTROL INPUTS ($P_{\text{AVG}} = W/T$) (MPC ODE45 CONTAINS THE ODE45 SIMULATED COST RESULTING FROM THE SAMPLED MPC INPUT)

Figure 9 shows the state, input and power trajectories for the wave moment M_{e1}. The MPC input is plotted as a staircase, as it is applied in this way. It can be seen that the MPC strategy and the optimal strategy are quite similar. The main difference is in the singular arcs, where the MPC does not show the discontinuous behavior (it resembles behavior similar to the fmincon plot in Figure 4). This results in a different power flow in these regions. Figure 10 shows the same behaviour. The parts where constraints are active coincide, however the control strategy differs when constraints are not active. The reason for this is not clear, although we suspect that it has to do with either the discrete cost function approximation that is not exact, or the solver not finding the global maximum. We saw similar results when using a different NLP solver for the optimal control in Section IV-A that also failed to capture this discontinuity. Although the result is interesting and deserves further attention, the impact on produced power is small. The difference we see in power production can most likely be contributed to the shorter horizon of the MPC strategy.

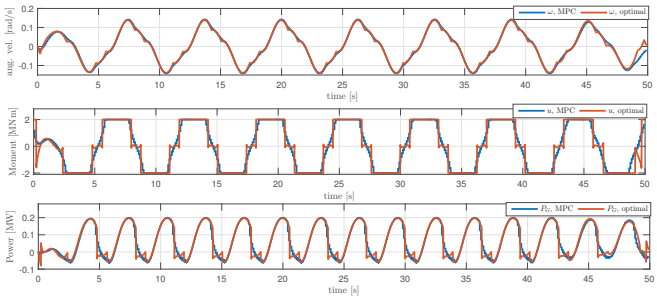

Fig. 9. Angular velocity reponse, control moment and generated power for the external wave moment M_{e1} (A perfect sine with an amplitude of 2 [MNm]). The resulting input contains both singular and bang arcs.

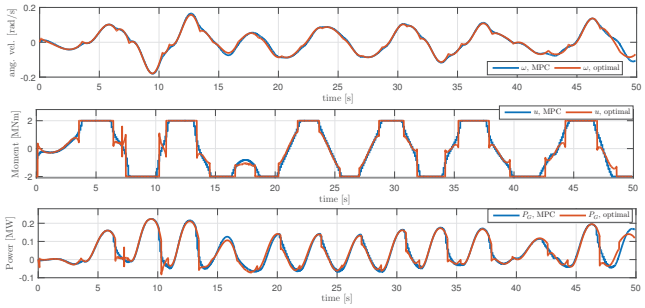

Fig. 10. Angular velocity response, control moment and generated power for the external wave moment M_{e3} (Measured sea state S3). The resulting input contains both singular and bang arcs.

In Figure 11 we show the simulation results for the external wave moment M_{e2}. This wave moment was used because it results in inactive constraints. It was found numerically impossible to completely remove the constraints for the optimal control simulation with ICLOCS. We see that the optimal control briefly touches a constraint and results in a sine wave with a constant torque shift. Apart from this shift, the resulting control strategies from the MPC and optimal simulation appear quite similar. Interestingly, MPC does result in a zero-mean torque. As one would physically expect, a static torque shift does not greatly influence the total energy generated, which also is illustrated in Figure 11. The qualitative difference in the MPC and optimal control may likely be contributed to the discretization and the shorter prediction horizon.

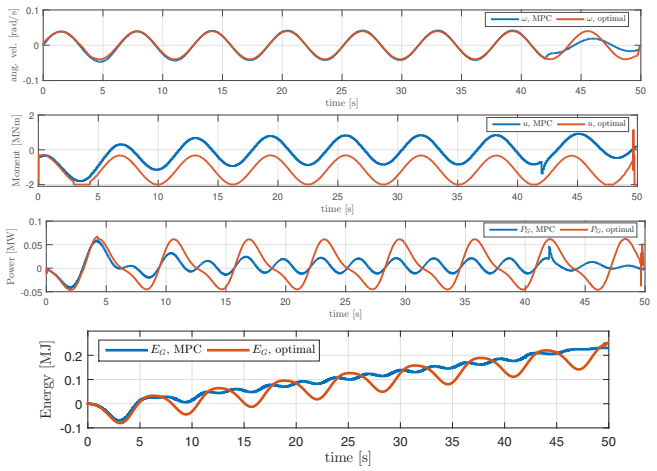

Fig. 11. Angular velocity response, control moment, generated power and energy for the external wave moment M_{e2} (A perfect sine with an amplitude of 0.5 [MNm]). The resulting input is totally singular.

VI. CONCLUSIONS

In this paper, we investigated the optimal control strategy of a wave energy converter in the presence of control torque constraints. We used a linearized model of the wave energy converter dynamics and implemented power take off friction loss in the harvested energy integral. We showed using Pontryagin's maximum principle that the optimal solution is singular-bang. To obtain a characterization of the singular solution we used higher order derivatives of the switching function and verified the result using the Generalized Legendre-Clebsch condition. We showed that the transitions from bang to singular subarcs are discontinuous. For this purpose, we used a state transformation to prove non-zeroness of the second time derivative of the switching function, reducing it to a simple observability test. We used these findings to verify the result of a numerical direct method. It was found that the numerical direct method was sensitive to the choice of NLP solver. The characterization of the singular solution and the proof of discontinuous singular-bang transitions validated that the numerical results are correct. It was found that the optimal control strategy in the presence of control torque constraint reverses power at certain intervals to optimize the total energy that is harvested. This is in line with the results for unconstrained optimal control found in literature.

The optimal control was used to validate an existing MPC strategy. It was found that the MPC strategy exhibits qualitatively different singular behavior than the optimal control. The impact of this difference on energy production was determined for various wave signals and was found to be small. The MPC strategy performs very well and in all cases harvests at least 92% (86%) of the energy. The difference between the optimal control and the MPC strategy is most likely due to the discretization of the cost function, or the solver failing to find the global optimum. More research is needed to give definitive conclusions. However, we can state that the optimal control problem for the linearized system with active constraints can be accurately solved. The MPC strategy shows performance close to this optimal control strategy and is therefore a very valid candidate for implementation. For practical purposes, future research should focus on more accurate models of the wave energy converter and the power take off friction. For theoretical purposes, the cause of the difference in singular behavior may be interesting. Furthermore, a challenge may lie in determining numerically reliable totally singular solutions from Pontryagin's principle, and translating these solutions to practically implementable control strategies.

REFERENCES

[1] J. Kofoed, P. Frigaard, and M. Kramer, "Recent developments on wave energy utilization in Denmark," *Proceedings of the Workshop on Renewable Ocean Energy Utilization*, 2006.

[2] A. Mütze and J. Vining, "Ocean wave energy conversion, a survey," *Proceedings of the 41st IEEE IAS Annual Conference*, vol. 3, pp. 1410–1417, 2006.

[3] J. Ringwood, G. Bacelli, and F. Fucso, "Energy-maximizing control of wave-energy converters," *IEEE control systems magazine*, vol. 34, no. 5, 2014.

[4] Wave Star A/S, "http://www.wavestarenergy.com."

[5] R. Hansen, T. Andersen, and H. Pedersen, "Model based design of efficient power take-off systems for wave energy converters," *The Twelfth Scandinavian International Conference on Fluid Power*, 2011.

[6] Z. Feng and E. C. Kerrigan, "Latching declutching control of wave energy converters using derivative-free optimization," *IEEE Transactions on Sustainable Energy*, vol. 6, no. 3, pp. 773 – 780, 2015.

[7] J. Barradas-Berglind *et al.*, "Energy capture optimization for an adaptive wave energy converter," in *Proceedings of the 2nd International Conference on Renewable Energies Offshore - RENEW 2016*, 2016.

[8] J. Falnes, "Optimum control of oscillation of wave-energy converters," *International Journal of Offshore and Polar Engineering*, 2002.

[9] S. Nielsen, Q. Qiang, M. Kramer, B. Basu, and Z. Zhang., "Optimal control of non-linear wave energy point converters," *Ocean engineering*, vol. 72, no. 11, 2013.

[10] G. Li, G. Weiss, M. Mueller, S. Townley, and M. R. Belmont, "Wave energy converter control by wave prediction and dynamic programming," *Renewable Energy*, vol. 48, pp. 392 – 403, 2012.

[11] E. Abraham and E. C. Kerrigan, "Optimal active control and optimization of a wave energy converter," *IEEE Transactions on Sustainable Energy*, vol. 4, no. 2, pp. 324 – 332, 2013.

[12] S. Zou, O. Abdelkhalik, R. Robinett, G. Bacelli, and D. Wilson, "Optimal control of wave energy converters," *Renewable Energy*, vol. 103, pp. 217 – 225, 2017.

[13] J. Hals, J. Falnes, and T. Moan, "Constrained optimal control of a heaving buoy wave-energy converter," *Journal of Offshore Mechanics and Arctic Engineering, ASME*, vol. 133, February 2011.

[14] P. Andersen, T. S. Pedersen, K. M. Nielsen, and E. Vidal, "Model predictive control of a wave energy converter," *IEEE Conference on Control Applications*, pp. 1540–1545, 2015.

[15] J. Mcdanell and W. Powers, "Necessary conditions for joining optimal singular and nonsingular subarcs," *Siam Journal of Control*, vol. 9, no. 2, 1971.

[16] P. Falugi, E. Kerrigan, and E. V. Wyk, "ICLOCS," 2010. [Online]. Available: http://www.ee.ic.ac.uk/ICLOCS

[17] W. Cummins, "The impulse response function and ship motions," *Schiffstechnick*, 1962.

[18] *Wamit user manual*, Wamit inc., Chestnut Hill, MA, 2002.

[19] H. J. Kelley, R. E. Kopp, and H. G. Moyer, "Singular extremals," in *Topics in Optimization*. Academic Press, 1967, pp. 63–101.

[20] O. von Stryk and R. Bulirsch, "Direct and indirect methods for trajectory optimization," *Annals of Operations Research*, vol. 37, 1992.

[21] A. Rao, "A survey of numerical methods for optimal control," *Advances in the astronautical Sciences*, vol. 135, no. 1, 2010.

[22] B. Houska, H. Ferreau, and M. Diehl, "ACADO Toolkit – An Open Source Framework for Automatic Control and Dynamic Optimization," *Optimal Control Applications and Methods*, vol. 32, no. 3, pp. 298–312, 2011.

[23] M. Diehl, "Lecture notes on optimal control and estimation," 2014.